
Towards Efficient Pareto Set Approximation via Mixture of Experts Based Model Fusion

Anke Tang
Wuhan University
Wuhan, China
anketang@whu.edu.cn

Li Shen
Sun Yat-sen University
Shenzhen, China
mathshenli@gmail.com

Yong Luo
Wuhan University
Wuhan, China
luoyong@whu.edu.cn

Shiwei Liu
University of Oxford
Oxford, UK
shiwei.liu@maths.ox.ac.uk

Han Hu
Beijing Institute of Technology
Beijing, China
hhu@bit.edu.cn

Bo Du
Wuhan University
Wuhan, China
dubo@whu.edu.cn

Abstract

Solving multi-objective optimization problems for large deep neural networks is a challenging task due to the complexity of the loss landscape and the expensive computational cost of training and evaluating models. Efficient Pareto front approximation of large models enables multi-objective optimization for various tasks such as multi-task learning and trade-off analysis. Existing algorithms for learning Pareto set, including (1) evolutionary, hypernetworks, and hypervolume-maximization methods, are computationally expensive and have restricted scalability to large models; (2) Scalarization algorithms, where a separate model is trained for each objective ray, which is inefficient for learning the entire Pareto set and fails to capture the objective trade-offs effectively. Inspired by the recent success of model merging, we propose a practical and scalable approach to Pareto set learning problem via mixture of experts (MoE) based model fusion. By ensembling the weights of specialized single-task models, the MoE module can effectively capture the trade-offs between multiple objectives and closely approximate the entire Pareto set of large neural networks. Once the routers are learned and a preference vector is set, the MoE module can be unloaded, thus no additional computational cost is introduced during inference. We conduct extensive experiments on vision and language tasks using large-scale models such as CLIP-ViT and GPT-2. The experimental results demonstrate that our method efficiently approximates the entire Pareto front of large models. Using only hundreds of trainable parameters of the MoE routers, our method even has lower memory usage compared to linear scalarization and algorithms that learn a single Pareto optimal solution, and are scalable to both the number of objectives and the size of the model. Our method significantly reduces the computational burden of learning the Pareto set, for example, in the two-task case, it can be achieved in just a few minutes. Code is available at: https://github.com/tanganke/pareto_set_learning

1 Introduction

Multi-objective optimization problems (MOOPs) are ubiquitous in machine learning, where multiple objectives need to be optimized simultaneously. The most related problem is multi-task learning, where a model learns a shared representation beneficial to all tasks by optimizing a joint objective function [39, 58]. Typically, this function is an equally weighted sum of task-specific objectives. However, conflicting objectives among tasks can lead to negative transfer, making finding a single

model that excels in all tasks challenging or impractical. In such scenarios, the Pareto set, containing all non-dominated solutions, is a better representation of the trade-offs between objectives [41, 5, 42]. A solution is said to be non-dominated if there is no other solution that is better in all objectives.

Existing Pareto set learning algorithms can be broadly divided into two primary categories depending on their ability to learn the entire Pareto set within a single run. The first category is capable of handling the MOOPs directly and can learn the entire Pareto set in a single run, but often struggle with the complexity of modern deep neural networks, such as evolutionary algorithms [10, 56], hypernetworks-based methods [34], and hypervolume maximization methods [3, 57]. The second category is exemplified by scalarization algorithms, such as linear scalarization and exact Pareto optimal search [32]. These methods transform a MOOP into a series of single-objective problems, each corresponding to a different combination of objective weights. However, the necessity to train a distinct model for each preference ray can be prohibitively resource-intensive.

However, the efficient learning of the Pareto set for large deep neural networks remains an open challenge due to the complexity of the loss landscape, which is characterized by a vast, high-dimensional parameter space and the inherent non-convexity of the optimization problem. This complexity makes it difficult to navigate towards a set of solutions that are non-dominated in all objectives. Moreover, the computational cost of training and evaluating large models is prohibitively expensive. Each iteration of training involves a substantial number of operations, including forward and backward passes through the network. The evaluation cost also scales up with the model size and the number of objectives. These challenges directly impact the scalability of existing algorithms, making them fail to learn the entire Pareto set for large models efficiently.

In this study, we propose a novel approach to efficiently approximate the entire Pareto set problem across multiple downstream tasks. Inspired by recent work on multi-task model merging [45], we adapt the weight-ensembling mixture of experts (MoE) structure to approximate the Pareto set of large neural networks, which is practical and scalable to both the number of objectives and the size of the model. Specifically, this approach can be broken down into three steps: (1) **model mixing**: we first mix different task-specific models into a single up-scaled MoE model, which captures a range of knowledge from all tasks. (2) **router fine-tuning**: we iteratively update the routers of the MoE module to learn the trade-offs between different objectives. At each step, we sample a preference vector randomly from the standard simplex and fine-tune the routers using gradient information. (3) **MoE unloading and inference**: once the routers are learned and a preference vector is set, the MoE modules can be unloaded, and no additional computational cost is introduced during inference.

The main contributions of this work are as follows:

- We propose a novel approach to efficiently approximate the entire Pareto set of large neural networks using a Pareto weight-ensembling mixture of experts (PWE MoE) structure.
- We introduce two training strategies, one based on linear scalarization and another based on exact Pareto optimal search that can effectively fine-tune the routers of MoE modules.
- We explore different up-scaling strategies, including using only the MLP modules or incorporating the Attention blocks as well, for the MoE-based model up-scaling process.
- We conduct extensive experiments on both vision and language tasks using large-scale models such as CLIP-ViT and GPT-2 to demonstrate the effectiveness of our method.

2 Related Work

Pareto set learning. One of the fundamental tasks in the multi-objective optimization problem is to learn the Pareto set, which comprises all non-dominated solutions offering trade-offs between objectives. Evolutionary algorithms [10, 56], hypervolume-maximization methods [3, 57], and multi-objective Bayesian optimization [28] are popular choices for approximating the Pareto set. Sener and Koltun [42] were among the first to explore Pareto optimality in the context of deep learning, employing the Multiple Gradient Descent Algorithm (MGDA) [11]. Pareto Multi-Task Learning (PMTL) [29], Exact Pareto Optimal (EPO) [32], and Impartial Multi-Task Learning (IMTL) [31] enable users to adjust the trade-off between objectives to specify their preferences. However, they can only identify a single Pareto optimal solution in a single run. Hypernetwork-based methods [34, 19] and manifold learning-based method [12] can scale to deep neural networks with a few million parameters and learn the entire Pareto set simultaneously.

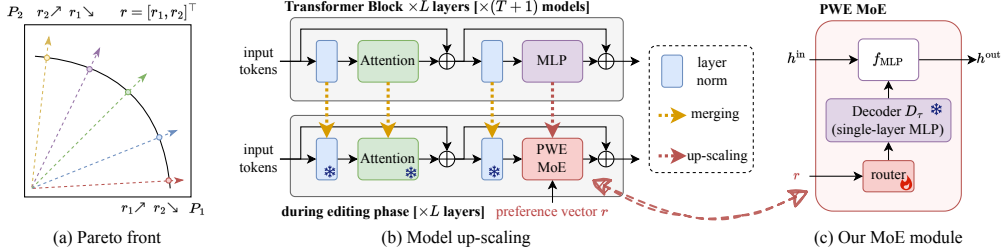


Figure 1: Overview. (a) An illustration of Pareto front learning in MOOP. Where P_1 and P_2 are performance metrics for two tasks, colored lines represent different Pareto optimal solutions, and the solid black line represents the Pareto front. (b) An overview of the model up-scaling process. We upcycle the MLP modules to MoE modules and merge the remaining parts using task arithmetic. (c) The MoE module, comprising a routing network and a parameter decoder network. The routing network accepts a user preference vector and generates routing weights for weight-ensembling.

Model fusion. Model merging is a highly effective and scalable approach to aggregating knowledge from multiple models into a unified model [59, 27]. A common practice to merge multiple models is by performing element-wise interpolation on weights, such as simple averaging [49, 7, 23, 40], task arithmetic [21, 17], and Fisher merging [33]. Other approaches such as mode connectivity-based methods [9, 13, 15, 14, 46, 54, 2], alignment-based methods [22, 30, 16, 1] are also crucial for effective model merging. A common challenge in model merging is task interference and parameter conflicts, which can be addressed through various approaches, such as subspace-based [53, 44], representation-based [52, 22], and parameter-based methods [51].

Our proposed method differs from existing model fusion approaches that usually integrate individual models into a single multi-task model. Instead, we merge multiple expert models to approximate the entire Pareto set. Additionally, our approach is the first to approximate the Pareto set through model merging, which is more efficient and scalable compared to existing Pareto set learning methods.

3 Reinterpreting Pareto Set Learning

In this section, we first introduce the formulation of Pareto set learning, then recast the Pareto set learning problem into the general framework of the model merging problem.

3.1 Preliminary

The challenge of multi-objective optimization problems (MOOP) stems from the conflicting objectives they present, resulting in a range of trade-off optimal solutions (referred to as Pareto optimal solutions) rather than a single optimal solution. Given a set of T objectives, each solution $\theta \in \mathbb{R}^N$ in the search space can be evaluated by a vector of T objective functions $l(\theta) = [l_1(\theta), l_2(\theta), \dots, l_T(\theta)]$. Before we delve into the details of our proposed method, we first introduce the concept of Pareto dominance, which is essential for comparing solutions in multi-objective optimization problems [4, 5].

Definition 3.1 (Pareto dominance). *We say that a solution θ_1 dominates another solution θ_2 , denoted as $\theta_1 \prec \theta_2$, if and only if $\forall t \in [T], l_t(\theta_1) \leq l_t(\theta_2)$ and $\exists t \in [T]$ such that $l_t(\theta_1) < l_t(\theta_2)$.*

Pareto dominance is transitive, which means that if $\theta_1 \prec \theta_2$ and $\theta_2 \prec \theta_3$, then $\theta_1 \prec \theta_3$.

Definition 3.2 (Pareto optimality, Pareto set, and Pareto front). *A solution θ is said to be Pareto optimal if there is no other solution that dominates it. The set of all Pareto optimal solutions is called the Pareto set, and the corresponding objective vectors are called the Pareto front.*

3.2 Pareto Set Learning as Multi-Task Model Merging Problem

A popular solution to seek Pareto optimal solution is linear scalarization (LS), which converts the multi-objective optimization problem into a single-objective optimization problem by linearly combining the objectives, i.e., $\min_{\theta} \sum_{t=1}^T r_t l_t(\theta)$, s.t. $\sum_{t=1}^T r_t = 1$ and $r_t > 0$, where r_t is the weight for the t -th objective and the vector $\mathbf{r} = [r_1, r_2, \dots, r_T]$ is denoted as the preference vector. We demonstrate the concept of the Pareto set/front using a two-task example, as shown in Figure 1(a). However, linear scalarization fails to capture the trade-offs between objectives and can only identify a single Pareto optimal solution along the convex part of the Pareto front [4, 34], and selecting an appropriate preference vector \mathbf{r} that accurately represents the user’s preferences can be challenging.

Existing methods for learning the entire Pareto front face challenges in scaling to large models. Pareto HyperNetwork is great and effective for small-scale models [34], but its practicality diminishes for larger models. This is because the output of the hypernetwork matches the number of parameters in the primary network. For instance, if the hypernetwork is a simple MLP with a single hidden layer of size $H = 100$, its parameter count would be $O(H \times N)$. Consequently, a small model with 10M parameters would necessitate a hypernetwork with 1B parameters. A possible compromise is to generate only a subset of the parameters and share the rest across the tasks. However, this would lead to a suboptimal solution, and the design of the hypernetwork would be nontrivial. Another intriguing approach is to learn a simplex Pareto subspace by learning a matrix of parameters $\Theta = [\theta_1, \theta_2, \dots, \theta_m]^T \in \mathbb{R}^{m \times N}$ and a task weighting matrix $\mathbf{W} \in \mathbb{R}^{m \times T}$ simultaneously [12]. However, the assumption of a linear mapping from parameter space to objective space may not be valid, resulting in an imbalanced distribution of Pareto optimal relative to the preference vector. Additionally, optimizing such a large parameter matrix Θ demands substantial memory and computational resources, resulting in poor scalability with respect to both the number of tasks and the size of the model.

Why do we opt to merge models? Considering the above challenges and limitations in scalability, capturing the trade-offs, and flexibility in selecting the preference vector, we opt to learn Pareto set by leveraging the inherent knowledge from different task-specific models instead of learning from scratch. Our key insights are: (1) each task-specific model can be viewed as a Pareto optimal corresponding to a special preference vector, e.g. $\mathbf{r} = [1, 0, 0, \dots, 0]$ for the first task. (2) The Pareto set can be approximated by interpolating between the task-specific models in the parameter space, which is more scalable and flexible than learning from scratch. (3) Merging models allow us to capture the trade-offs between objectives, even when the merging weights are non-convex. Formally, Given a set of models $\{\theta_i\}_{i=1}^T$, we can merge them into a single model $\theta_{\text{merged}} = \mathcal{A}(\{\theta_i\}_{i=1}^T, w)$, where \mathcal{A} is a merging algorithm, and w is the algorithmic parameters that control the merging process. To approximate the Pareto set, we can substitute the algorithmic parameters with a function of the preference vector, i.e., $w = R(\mathbf{r})$ where $R: \mathbb{R}^T \rightarrow \mathbb{R}^{|w|}$ can be an arbitrary nonlinear function. The resulting merged model θ_{merged} is then a function of the preference vector \mathbf{r} as follows:

$$\theta_{\text{merged}} = \mathcal{A}(\{\theta_i\}_{i=1}^T, R(\mathbf{r})). \quad (1)$$

4 Efficient Pareto Set Approximation via MoE-Based Model Fusion

Inspired by recent advances in multi-task model merging [27, 45], we propose an MoE-based approach to approximate the entire Pareto front of large models via weight-ensembling. Our method is scalable to both the number of objectives and the size of the model, and significantly reduces the computational demand, consuming even less memory compared to linear scalarization.

4.1 MoE-Based Model Up-Scaling and Pareto Set Approximation

Given T task-specific models $\{\theta_i\}_{i=1}^T$ that are fine-tuned from a common pre-trained model θ_0 , we upscale the model by incorporating our proposed MoE module, which handles objective trade-offs, as shown in Figure 1(b). To make the notation concise, we denote the part of parameters that are to be up-scaled as $\phi_0, \phi_1, \dots, \phi_T$, where ϕ_0 and ϕ_i represent the parameters of the pre-trained model and the i -th task-specific model, respectively. The remaining parts that do not up-scale are merged using task arithmetic, which is a straightforward, effective, and scalable element-wise operation. Similarly, we denote these parameters as $\psi_0, \psi_1, \dots, \psi_T$, the merged parameters are $\psi^* = \psi_0 + \lambda \sum_{t=1}^T \psi_t$. Where λ is a scalar scaling coefficient selected on a validation set. We also discuss this partial up-scaling strategy, along with another strategy that up-scales Attention blocks as well.

The Pareto Weight-Ensembling Mixture of Experts (PWE MoE) module. Figure 1(c) shows the proposed PWE MoE module, which includes a routing network $R: \mathbb{R}^T \rightarrow \mathbb{R}^T$, which is a nonlinear mapping, and a parameter decoder $\mathbb{R}^T \mapsto \mathbb{R}^{|\phi|}$, and a realization function $F: \mathbb{R}^{|\phi|} \mapsto \mathcal{F}$, mapping the parameters to function space of the up-scaled module. The routing network takes a user preference vector \mathbf{r} as input and generates routing weights for weight-ensembling. These routing weights are then used by the parameter decoder network to generate the parameters for the realization function. The decoder network itself is a fixed linear layer. The MoE is described mathematically as:

$$w = R(\mathbf{r}), \phi^* = \mathbf{D}_\tau w + \phi_0, h^{\text{out}} = F(\phi^*)(h^{\text{in}}), \quad (2)$$

where $\mathbf{D}_\tau \in \mathbb{R}^{|\phi| \times T}$ is a dictionary matrix that contains the task vectors of the up-scaled module, $\mathbf{D}_\tau = [\tau_1, \tau_2, \dots, \tau_T]$ and $\tau_i = \phi_i - \phi_0$, h^{in} and h^{out} are the input and output sequence of tokens.

The major difference between the proposed PWE MoE module and the weight-ensembling MoE from Tang et al. [45] is that our routing network R takes the preference vector \mathbf{r} as input, which allows the MoE module to generate parameters based on user preference and can be unloaded. This is highlighted in Figures 1(b) and 1(c). In contrast, the original weight-ensembling MoE generates routing weights based on input data, aiming to adapt to the input data distribution.

Approximation of the Pareto set. Given a MOOP with T objectives, the Pareto front is defined as $\mathcal{P} = \{\mathcal{L}(\phi) \mid \phi \in \Phi \text{ and } \nexists \phi' \in \Phi \text{ s.t. } \phi' \prec \phi\}$, where $\mathcal{L}(\phi) = (l_1(\phi), \dots, l_T(\phi))$ is the vector of task-specific losses, and $\Phi = \mathbb{R}^{|\phi|}$ is the space of parameters ϕ for the upscaled module.

The proposed PWE MoE module searches a subspace of the parameter space that is the span of the task vectors centered at pre-trained weights, rather than the entire parameter space. This is a reasonable assumption, as the Pareto front is often a convex set. Let $\Phi_{\text{MoE}} = \{\phi \mid \phi = \mathbf{D}_\tau w + \phi_0, w \in \mathbb{R}^T\}$ be the subspace of Φ that can be represented by the proposed MoE model, we have $\Phi_{\text{MoE}} \subset \Phi$. We can also define the Pareto front of the MoE model as a function of the preference vector \mathbf{r} as follows:

$$\mathcal{P}_{\text{MoE}} = \left\{ \mathcal{L}'(\mathbf{r}) \mid \mathcal{L}'(\mathbf{r}) = \mathcal{L}(\mathbf{D}_\tau R(\mathbf{r}) + \phi_0), \mathbf{r} \in \Delta^{T-1} \text{ and } \nexists \mathbf{r}' \in \Delta^{T-1} \text{ s.t. } \mathcal{L}'(\mathbf{r}') \prec \mathcal{L}'(\mathbf{r}) \right\}. \quad (3)$$

In other words, the Pareto front of the MoE model is the set of loss vectors achieved by the MoE model for all possible preference vectors \mathbf{r} in the $(T - 1)$ -dimensional simplex, such that no other preference vector achieves a loss vector that Pareto dominates it. To further establish the connection between the Pareto front and the MoE Pareto front, we provide a theoretical analysis, which guarantees that the MoE module can approximate the Pareto front of the up-scaled model with a bounded error.

Theorem 4.1 (Existence of an error bound, proved in Appendix A). *Similar to the true Pareto front \mathcal{P} , let $\mathcal{P}_{\text{MoE}} = \{\mathcal{L}(\phi) \mid \phi \in \Phi_{\text{MoE}} \text{ and } \nexists \phi' \in \Phi_{\text{MoE}} \text{ s.t. } \phi' \prec \phi\}$ be the Pareto front estimated by the proposed MoE module. Assume that the loss functions $\{l_t\}_{t=1}^T$ are continuous, then for any $\mathcal{L}(\phi^*) \in \mathcal{P}_{\text{MoE}}$, there exists an $\mathcal{L}(\phi) \in \mathcal{P}$ and an $\epsilon > 0$ such that $\|\mathcal{L}(\phi^*) - \mathcal{L}(\phi)\|_2 \leq \sqrt{T}\epsilon$.*

Furthermore, if each loss function l_t is Lipschitz continuous with constant L_t , i.e. $\|l_t(\phi) - l_t(\phi')\| \leq L_t \|\phi - \phi'\|_2$ for all $\phi, \phi' \in \Phi$, then we can take $L = \sup\{L_t\}_{t=1}^T$ and obtain the following bound:

$$\|\mathcal{L}(\phi^*) - \mathcal{L}(\phi)\|_2 \leq \sqrt{T}L\|\phi^* - \phi\|_2. \quad (4)$$

However, determining the Lipschitz constants of the loss functions is non-trivial and depends on the specific model and task. In practice, the value of ϵ is less important than the fact that it exists and can be made arbitrarily small by increasing the density of the MoE subspace Φ_{MoE} within the entire parameter space Φ . This density can be controlled by factors such as the number of models to be up-scaled and the diversity of the task vectors. In addition to the theoretical guarantee, we have:

Remark 4.1 (Scalability). *The number of trainable parameters in the MoE module scales linearly with the number of tasks and is independent of the width of the pre-trained model. This allows efficient scaling to a large number of tasks without significantly increasing memory usage.*

Remark 4.2 (computational efficiency). *Because the routing weight vector w depends only on the preference vector \mathbf{r} , the MoE module can be unloaded by substituting the MoE module with $F(\phi^*)$ after setting a preference vector, and no additional computational cost is introduced during inference.*

Two up-scaling strategies. We discuss two up-scaling strategies: one that only uses the MLP modules and another that incorporates the Attention blocks. The choice of up-scaling strategy affects the quality of the Pareto set approximation and the computational demands. A more fine-grained up-scaling strategy leads to better approximation but increases the number of trainable parameters in the routers. To obtain a more comprehensive understanding of different strategies, we further investigate the similarity of Attention blocks and MLP modules in parameter space.

To establish a qualitative understanding of ‘‘similarity’’ in parameter space, we consider two functions are similar if they have similar outputs for similar inputs. This definition can be extended to the parameter space of neural networks. To quantify this discrepancy, we Taylor expand the function $f(\cdot, \phi)$ around pretrained weights ϕ_0 :

$$f(\cdot, \phi) = f(\cdot, \phi_0) + \nabla_\phi f(\cdot, \phi_0)^\top (\phi - \phi_0) + O(\|\phi - \phi_0\|^2). \quad (5)$$

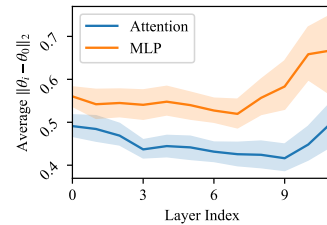


Figure 2: The L_2 norm of the delta parameters of CLIP.

Where ϕ are the weights after fine-tuning. For a given input x , the output of the function can be linearly approximated around ϕ_0 since $\nabla_{\phi} f(x, \phi_0)$ is a constant vector. So $\|f(x, \phi_1) - f(x, \phi_2)\|_2 \propto \|\phi_1 - \phi_2\|_2$ for ϕ_1, ϕ_2 close to ϕ_0 . Therefore, the Euclidean distance in the parameter space is a good approximation of the functional discrepancy [45, 25]. Figure 2 shows that Attention blocks are more similar to each other than MLPs, suggesting that up-scaling the MLPs may be more beneficial, as the MLPs are more diverse and thus task-specific.

Structure design and parameter initialization of the routers. We implement the routing networks as fully connected feed-forward neural networks with a single hidden layer of size $2T$. The hidden layer is followed by a ReLU activation function. Mathematically, the routers are defined as $R(\mathbf{r}) = \mathbf{W}_2 \text{ReLU}(\mathbf{W}_1 \mathbf{r} + \mathbf{b}_1) + \mathbf{b}_2$, where the weights \mathbf{W}_1 and \mathbf{W}_2 are initialized using the Gaussian distribution with zero mean and standard deviation of 0.01, and the bias \mathbf{b}_1 is initialized to zero, and \mathbf{b}_2 is initialized to λ , where λ is a same scalar scaling coefficient used in the task arithmetic. After this initialization setup, routers are encouraged to output an initial routing weight vector that is close to the task arithmetic.

4.2 Model Training

Once the model is merged and up-scaled, the routers of MoE modules undergo fine-tuning as described in Algorithm 1. During this fine-tuning process, we uniformly sample \mathbf{r} from the $(T-1)$ -simplex at each iteration, equivalent to sampling from a Dirichlet distribution with a concentration parameter α , which is set to 1 in our experiments. We then merge the MoE models with the given preference vector. The loss function L is computed in the same manner as linear scalarization (LS) or the expected Pareto optimal (EPO). Then the routers are updated using the gradient descent method. This process is repeated until the routers converge.

The number of trainable parameters depends on the number of tasks and the extent to which the model is up-scaled, typically ranging from hundreds to thousands. Compared to full fine-tuning, the number of parameters is quite low. This results in our method having relatively low memory usage, even lower than linear scalarization. In Table 8, we summarize the device states during training.

5 Experiments

In this section, we conduct experiments on a variety of tasks, including image classification and text generation to demonstrate the effectiveness and scalability of our method. Our experiments are conducted on two classes of large SOTA models: CLIP-ViT [38] for image classification tasks and GPT-2 [37] for text generation tasks, with up to eight objectives. In terms of computational resources, our method requires only a few minutes to estimate the entire Pareto set. Code for reproduction is available at https://github.com/tanganke/pareto_set_learning.

Baseline methods. We compare our method with the following baseline Pareto set learning methods: Single Task Learning (STL), LS, EPO [32], and MGDA [42]. In addition, we compare our method with several multi-task model merging methods, including Weight Averaging [49], Fisher Merging [33], RegMean [22], Task Arithmetic [21], and Ties-Merging [51].

5.1 Open-Vocabulary Image Classification

We first evaluate our method on open-vocabulary image classification tasks using the CLIP models, which are pre-trained on large-scale image-text pairs. We consider eight downstream tasks

Algorithm 1 Router fine-tuning

```

1: while not converged do
2:    $\mathbf{r} \sim \text{Dir}(\alpha = 1)$ 
3:   for  $m$  in all MoE modules do
4:      $\phi^* \leftarrow \mathbf{D}_\tau R(\mathbf{r}) + \phi_0$   $\triangleright$  Merge
5:     unload  $m$  to  $F(\phi^*)$ 
6:   end for
7:   for each task  $t$  do
8:     sample a batch of data  $B_t \sim \mathcal{D}_t$ 
9:     compute the loss  $l_t$  on  $B_t$ 
10:  end for
11:  if LS then
12:     $L \leftarrow \sum_{t=1}^T r_t l_t$ 
13:  else if EPO then
14:     $L \leftarrow \text{EPO}(\theta_R, \{l_t\}_{t=1}^T, \mathbf{r})$ 
15:  end if
16:   $\theta_R \leftarrow \theta_R - \eta \nabla_{\theta_R} L$ 
17:  reset MoE modules
18: end while

```

Table 1: Partial summarization of device specification for two-task Pareto set learning using CLIP-ViT-B/32. Full details are provided in Table 8.

Method	GPU usage	Wall Time
LS	3.4GB	\approx 4 mins
EPO	6.1GB	\approx 8 mins
Ours-LS	2.8GB	\approx 2-3 mins
Ours-LS (All)	3.9GB	\approx 3 mins
Ours-EPO	3.1GB	\approx 3-4 mins
Ours-EPO (All)	3.9GB	\approx 5-6 mins

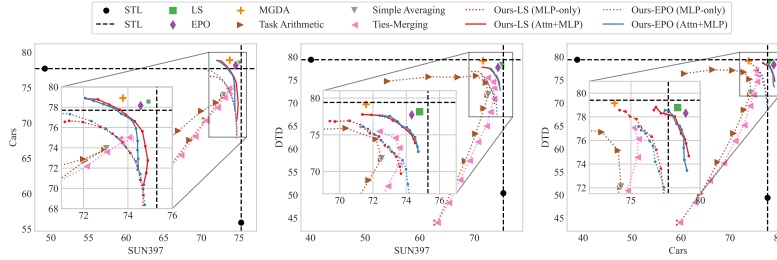


Figure 3: Visualization of results for two image classification tasks using CLIP-ViT-B/32.

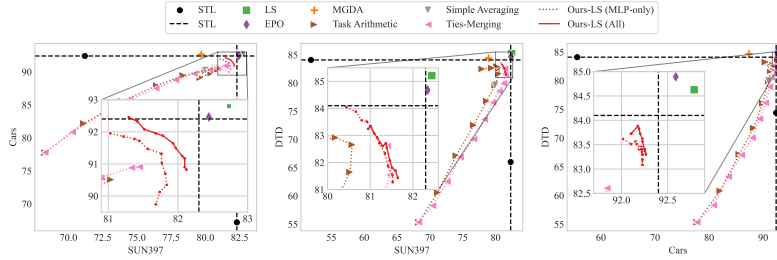


Figure 4: Visualization of results for two image classification tasks using CLIP-ViT-L/14.

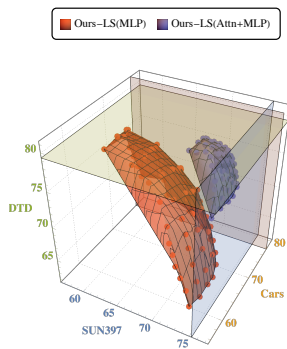
spanning various data domains, including SUN397 [50], Stanford Cars [24], RESISC45 [6], EuroSAT [18], SVHN [35], GTSRB [43], MNIST [26] and DTD [8]. A summarization of computational requirements is provided in Tables 1 and 8, demonstrating the computational efficiency of our method.

Pairs of tasks. Initially, we focus on Pareto set learning for two tasks, selecting the SUN397-Cars, SUN397-DTD, and Cars-DTD pairs for assessment. We visualize the results using CLIP-ViT-B/32 and CLIP-ViT-L/14 in Figures 3 and 4, respectively. The horizontal and vertical axes represent the accuracy of the first and second tasks, respectively. For Task Arithmetic and Ties-Merging, we show the results with different scaling factor. We have the following key observations:

1. For CLIP-ViT-B/32 models, joint fine-tuning on SUN397-Cars and Cars-DTD improves performance on Cars but worsens it on SUN397 and DTD, suggesting a one-way positive transfer to Cars. Joint tuning on SUN397 and DTD negatively impacts both, showing a negative transfer effect. *Negative transfer is a common issue in multi-task learning.*
2. For CLIP-ViT-L/14 models, performance improvements are generally positive for LS and EPO, highlighting that *the larger model size enhances robustness to task interference.*
3. Our method is able to successfully approximate the Pareto set, *providing an good trade-off between the two tasks.* Ours-LS shows similar performance to Ours-EPO.
4. For CLIP-ViT-B/32, up-scaling both the MLP and Attention leads to consistently better performance. However, for CLIP-ViT-L/14, gains from scaling both components are similar, showing that *the benefits of up-scaling Attention are less significant in larger models.*
5. Non-dominant points on the Task Arithmetic curves mainly appear in the middle, whereas the Ties-Merging curves are near the endpoints. This indicates that *Ties-Merging is more effective at resolving task interference compared to Task Arithmetic*, aligning with the observations in Figure. 7, where Ties-Merging consistently increases the average accuracy.

Three tasks. We further extend our experiments to three tasks using the SUN397-Cars-DTD triplet. In Figure 5(a), we visualize the 3D view of Pareto front for Ours-LS (MLP) and Ours-LS (Attn+MLP) using CLIP-ViT-B/32. We uniformly sample preference vectors from the standard 2-dimensional simplex, generate parameters for the primary model and evaluate on the three tasks. It is observed that the Pareto front is convex, and the uniformly sampled points are distributed nearly uniformly across the front. The points on Ours-LS (Attn+MLP) generally dominate those on Ours-LS (MLP), indicating that *up-scaling both components can improve the approximation of the Pareto front.* Figure 5(b) is a performance comparison table of different methods, utilizing an equal-weight preference vector and three special unit preference vectors. Here are some key observations from the table:

1. Fine-tuned (STL) models achieve the highest average accuracy of 77.5% across the three tasks. They are served as the upper bounds of the single task accuracies here.



(a)

Method	SUN397	Cars	DTD	Avg.
Pretrained	63.2	59.2	44.4	55.6
Fine-tuned (STL)	75.3	77.7	79.4	77.5
LS (equal-weight)	75.1	77.2	78.9	77.1
EPO (equal-weight)	74.3	78.6	77.7	76.9
MGDA	68.9	65.7	79.5	71.4
Weight Averaging	70.1	69.7	64.9	68.2
Task Arithmetic	70.1	70.6	67.6	69.4
Ties-Merging	71.3	71.2	67.7	70.1
Ours-LS (MLP,EW)	69.4	68.8	72.6	70.3
Ours-LS (Attn+MLP,EW)	71.7	74.7	76.1	74.2
Ours-LS (Attn+MLP,[1, 0, 0])	73.3	65.7	71.7	70.2
Ours-LS (Attn+MLP,[0, 1, 0])	69.1	77.9	71.3	72.8
Ours-LS (Attn+MLP,[0, 0, 1])	68.2	70.4	77.1	71.9

(b)

Figure 5: (a) The 3D visualization of the Pareto front using CLIP-ViT-B/32 models. The planes represent the fine-tuned models. (b) The performance comparison table of different methods.

Table 2: Multi-task performance comparison on eight image classification tasks using CLIP-ViT-B/32.

Method	SUN397	Cars	RESISC45	EuroSAT	SVHN	GTSRB	MNIST	DTD	Avg.
Pretrained	63.2	59.2	60.2	45.0	31.6	32.6	48.3	44.4	48.1
Fine-tuned (STL)	75.3	77.7	96.1	99.9	97.5	98.7	99.7	79.4	90.5
LS (equal-weight)	73.9	74.4	93.9	98.2	95.8	98.9	99.5	77.9	88.9
EPO (equal-weight)	74.2	78.3	93.4	98.2	95.7	97.3	99.0	78.0	89.3
MGDA	64.8	63.7	87.7	92.3	90.8	98.4	99.0	74.7	83.9
Weight Averaging	65.3	63.3	71.4	73.6	64.2	52.8	87.5	50.1	66.0
Fisher Merging	68.6	69.2	70.7	66.4	72.9	51.1	87.9	59.9	68.3
RegMean	65.3	63.5	75.6	78.6	78.1	67.4	93.7	52.0	71.8
Task Arithmetic	55.3	54.9	66.7	77.4	80.2	69.7	97.3	50.1	69.0
Ties-Merging	65.0	64.3	74.7	76.8	81.3	69.4	96.5	54.3	72.8
Ours-LS (MLP)	63.5	64.0	79.1	87.3	84.8	81.8	93.1	63.6	77.2
Ours-LS (Attn+MLP)	69.2	71.4	85.3	92.8	90.3	89.7	97.1	71.9	83.5
Ours-EPO (MLP)	66.2	65.9	77.5	82.7	81.6	79.4	88.2	64.3	75.7
Ours-EPO (Attn+MLP)	70.0	72.2	85.0	90.7	90.9	87.2	94.0	70.6	82.6

2. Among model merging methods, Ours-LS(Attn+MLP) outperforms other model merging methods with the highest average accuracy of 74.2%, followed by Ours-LS(MLP) at 70.3%.
3. Among model merging methods, when using Ours-LS (Attn+MLP) with unit preference vectors, the model achieves the highest accuracies on individual tasks. This demonstrates that by adjusting the preference vector, it can control the trade-off between objectives.

Scale up to eight tasks. We also broaden our experiments to include all eight downstream tasks. Due to the difficulty of visualizing the results in higher dimensions, we present the performance comparison in Tables 2 and 3 for CLIP-ViT-B/32 and CLIP-ViT-L/14, respectively. For fine-tuned models, we report the task performance for each individual task, whereas for other methods, we report the performance using the same backbone. In particular, for our method, we choose an equal-weight preference vector of $[\frac{1}{8}, \dots, \frac{1}{8}]^\top$ to assess the multi-task performance. The results of EPO and MGDA for CLIP-ViT-L/14 are not presented due to unsuccessful attempts to fine-tune the model with no more than 4×4090 GPUs due to insufficient GPU memory with batch size set to 12 per task.

We observe that (1) model merging methods generally have lower average accuracies compared to multi-task learning methods. (2) Moreover, the proposed methods, Ours-LS (MLP), Ours-LS (Attn+MLP), Ours-EPO (MLP), and Ours-EPO (Attn+MLP), outperform model merging baseline methods on both CLIP-ViT-B/32 and CLIP-ViT-L/14. (3) As the model size grows, the performance gap between multi-task learning methods and model merging methods narrows, indicating that *task arithmetic is an emerging property of large models*. This is consistent with the conclusion in [17]. (4) Only up-scaling the MLP modules outperforms the other model merging methods, up-scaling both the Attention and MLP modules further improves the performance.

Routing analysis. In order to gain deeper insight into the MoE modules’ routing mechanism, we conduct an examination of the expert routing weights associated with various preference vectors, utilizing CLIP-ViT-B/32 (Ours-LS, MLP only). For every unit preference vector, we calculate the routing weights at various depths for the MoE routers and display these weights in Figure 8. Notably, we have (1) *variability across depths*. The routing weights vary significantly across different depths

Table 3: Multi-task performance comparison on eight image classification tasks using CLIP-ViT-L/14.

Method	SUN397	Cars	RESISC45	EuroSAT	SVHN	GTSRB	MNIST	DTD	Avg.
Pretrained	68.2	77.9	71.3	61.3	58.4	50.6	76.4	55.4	64.9
Fine-tuned (STL)	82.3	92.4	97.4	99.9	98.1	99.2	99.7	84.1	94.1
LS (equal-weight)	80.8	90.6	96.3	96.3	97.6	99.1	99.6	84.4	93.5
Weight Averaging	72.1	81.6	82.6	91.4	78.2	70.6	97.0	62.8	79.5
Fisher Merging	69.2	88.6	87.5	93.5	80.6	74.8	93.3	70.0	82.2
RegMean	73.3	81.8	86.1	97.0	88.0	84.2	98.5	60.8	83.7
Task Arithmetic	74.1	82.1	86.7	92.6	87.9	86.8	98.9	65.6	84.4
Ties-Merging	75.0	84.5	88.0	94.3	85.7	82.1	98.7	67.7	84.5
Ours-LS (MLP)	77.6	88.5	92.5	96.1	95.2	94.7	98.2	79.1	90.2

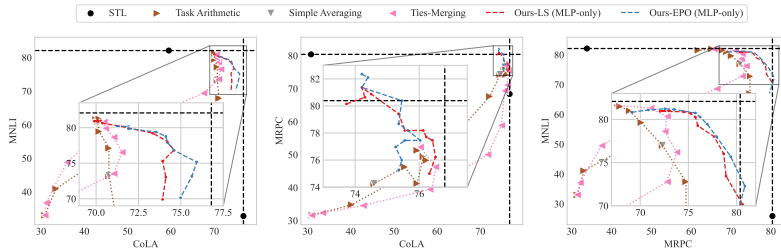


Figure 6: Visualization of results for natural language task pair experiments using GPT-2.

Table 4: Multi-task performance comparison on seven natural language tasks using GPT-2.

Method	MRPC	MNLI	COLA	SST-2	QNLI	QQP	RTE	Avg.
Fine-tuned (STL)	80.4	82.1	76.8	93.2	91.3	89.3	70.3	83.9
Simple Average	55.0	55.1	51.0	57.6	76.7	44.8	52.5	56.1
Task Arithmetic	67.9	68.1	68.8	85.1	70.1	80.9	47.3	69.4
Ties-Merging	68.4	71.4	68.4	81.8	69.6	82.4	47.7	70.0
Ours-LS (MLP)	77.0	68.8	72.5	85.2	75.6	81.1	62.8	74.7

of the model. (2) *Specificity to tasks*. Each preference vector, tied to a specific task, guides the routing towards relevant experts at higher depths. This shows the model’s ability to adjust its weights according to the preference vector, confirming the intended behavior of MoE to specialize expert usage per task. (3) *Expert utilization*. Certain experts are utilized more often across various preference vectors, and this usage varies at different depths. For instance, the ‘Cars’ expert is commonly used in early layers, suggesting its proficiency in extracting basic image features. Conversely, the ‘DTD’ expert is often used in later layers, indicating its specialization in deeper contextual understanding.

5.2 Natural Language Tasks

In addition to image classification tasks, we also evaluate our method on natural language tasks using GPT-2 models. (1) We first consider three task pairs from GLUE benchmark [47], including CoLA-MNLI, CoLA-MRPC, and MRPC-MNLI. We visualize the results using in Figure 6. It shows a similar pattern to the image classification task pair experiments, where our approach successfully approximates the Pareto set, offering a good trade-off between the pair of tasks. (2) We also scale up the number of objectives to seven and compare the results of an equal-weight preference vector with three model merging methods, Simple Averaging, Task Arithmetic and Ties-Merging, in Table 4.

6 Conclusion, Limitations, and Broader Impact

In this work, we have introduced a novel approach that addresses the limitations of previous methods that either find a single Pareto optimal solution or require extensive computational resources to identify the entire Pareto set. Our method, which leverages the weight-ensembling mixture of experts (MoE) structure, not only finds the Pareto set but also offers scalability to both the number of objectives and the size of the model. By ensembling the weights of specialized single-task models, the MoE module can effectively capture the trade-offs between multiple objectives and provide a close approximation of the entire Pareto set of large neural networks.

Limitations. Currently, our experiments are limited to Transformer-based models, such as ViT models and Transformer-based LLMs, further exploration can be conducted on other types of models, such as RNNs and CNNs, in future work. While the method aims to approximate the Pareto front using

a simple MLP-based MoE router, it may not always provide a complete or accurate representation of the Pareto set, further exploration can be conducted on more sophisticated router architectures.

Broader Impact. By enabling users to adjust trade-offs between objectives and identify Pareto optimal solutions, this method can improve decision-making processes. Moreover, the efficient nature of model merging methods can also reduce the computational burden of developing multi-task models. However, the deployment of highly capable models can lead to job displacement in certain sectors.

References

- [1] Samuel K. Ainsworth, Jonathan Hayase, and Siddhartha Srinivasa. Git Re-Basin: Merging Models modulo Permutation Symmetries, March 2023. URL <http://arxiv.org/abs/2209.04836>.
- [2] Gregory W. Benton, Wesley J. Maddox, Sanae Lotfi, and Andrew Gordon Wilson. Loss Surface Simplexes for Mode Connecting Volumes and Fast Ensembling, November 2021. URL <http://arxiv.org/abs/2102.13042>.
- [3] Nicola Beume, Boris Naujoks, and Michael Emmerich. SMS-EMOA: Multiobjective selection based on dominated hypervolume. *European Journal of Operational Research*, 181(3):1653–1669, September 2007. ISSN 0377-2217. doi: 10.1016/j.ejor.2006.08.008. URL <https://www.sciencedirect.com/science/article/pii/S0377221706005443>.
- [4] Stephen P. Boyd and Lieven Vandenberghe. *Convex Optimization*. Cambridge University Press, Cambridge, UK ; New York, 2004. ISBN 978-0-521-83378-3.
- [5] Edmund K. Burke and Graham Kendall, editors. *Search Methodologies: Introductory Tutorials in Optimization and Decision Support Techniques*. Springer US, Boston, MA, 2014. ISBN 978-1-4614-6939-1 978-1-4614-6940-7. doi: 10.1007/978-1-4614-6940-7. URL <https://link.springer.com/10.1007/978-1-4614-6940-7>.
- [6] Gong Cheng, Junwei Han, and Xiaoqiang Lu. Remote Sensing Image Scene Classification: Benchmark and State of the Art. *Proceedings of the IEEE*, 105(10):1865–1883, October 2017. ISSN 0018-9219, 1558-2256. doi: 10.1109/JPROC.2017.2675998. URL <http://arxiv.org/abs/1703.00121>. arXiv:1703.00121 [cs].
- [7] Alexandra Chronopoulou, Matthew E. Peters, Alexander Fraser, and Jesse Dodge. AdapterSoup: Weight Averaging to Improve Generalization of Pretrained Language Models, March 2023. URL <http://arxiv.org/abs/2302.07027>.
- [8] Mircea Cimpoi, Subhansu Maji, Iasonas Kokkinos, Sammy Mohamed, and Andrea Vedaldi. Describing Textures in the Wild. In *2014 IEEE Conference on Computer Vision and Pattern Recognition*, pages 3606–3613, Columbus, OH, USA, June 2014. IEEE. ISBN 978-1-4799-5118-5. doi: 10.1109/CVPR.2014.461. URL <https://ieeexplore.ieee.org/document/6909856>.
- [9] C. Daniel Freeman and Joan Bruna. Topology and geometry of half-rectified network optimization: 5th International Conference on Learning Representations, ICLR 2017. 2017. URL <http://www.scopus.com/inward/record.url?scp=85064823226&partnerID=8YFLogxK>.
- [10] K. Deb, A. Pratap, S. Agarwal, and T. Meyarivan. A fast and elitist multiobjective genetic algorithm: NSGA-II. *IEEE Transactions on Evolutionary Computation*, 6(2):182–197, April 2002. ISSN 1089778X. doi: 10.1109/4235.996017. URL <http://ieeexplore.ieee.org/document/996017/>.
- [11] Jean-Antoine Désidéri. Multiple-gradient descent algorithm (MGDA) for multiobjective optimization. *Comptes Rendus Mathématique*, 350(5):313–318, March 2012. ISSN 1631-073X. doi: 10.1016/j.crma.2012.03.014. URL <https://www.sciencedirect.com/science/article/pii/S1631073X12000738>.
- [12] Nikolaos Dimitriadis, Pascal Frossard, and François Fleuret. Pareto Manifold Learning: Tackling multiple tasks via ensembles of single-task models. In *Proceedings of the 40th International Conference on Machine Learning*, pages 8015–8052. PMLR, July 2023. URL <https://proceedings.mlr.press/v202/dimitriadis23a.html>.

- [13] Felix Draxler, Kambis Veschgini, Manfred Salmhofer, and Fred A. Hamprecht. Essentially No Barriers in Neural Network Energy Landscape, February 2019. URL <http://arxiv.org/abs/1803.00885>.
- [14] Rahim Entezari, Hanie Sedghi, Olga Saukh, and Behnam Neyshabur. The Role of Permutation Invariance in Linear Mode Connectivity of Neural Networks, July 2022. URL <http://arxiv.org/abs/2110.06296>.
- [15] Jonathan Frankle, Gintare Karolina Dziugaite, Daniel M. Roy, and Michael Carbin. Linear Mode Connectivity and the Lottery Ticket Hypothesis, July 2020. URL <http://arxiv.org/abs/1912.05671>.
- [16] George Stoica, Daniel Bolya, Jakob Bjorner, Taylor Hearn, and Judy Hoffman. ZipIt! Merging Models from Different Tasks without Training, May 2023. URL <http://arxiv.org/abs/2305.03053>.
- [17] Guillermo Ortiz-Jimenez, Alessandro Favero, and Pascal Frossard. Task Arithmetic in the Tangent Space: Improved Editing of Pre-Trained Models, May 2023. URL <http://arxiv.org/abs/2305.12827>.
- [18] Patrick Helber, Benjamin Bischke, Andreas Dengel, and Damian Borth. Introducing eurosat: A novel dataset and deep learning benchmark for land use and land cover classification. In *IGARSS 2018-2018 IEEE International Geoscience and Remote Sensing Symposium*, pages 204–207. IEEE, 2018.
- [19] Long P. Hoang, Dung D. Le, Tran Anh Tuan, and Tran Ngoc Thang. Improving Pareto Front Learning via Multi-Sample Hypernetworks. *Proceedings of the AAAI Conference on Artificial Intelligence*, 37(7):7875–7883, June 2023. ISSN 2374-3468, 2159-5399. doi: 10.1609/aaai.v37i7.25953. URL <https://ojs.aaai.org/index.php/AAAI/article/view/25953>.
- [20] Gabriel Ilharco, Mitchell Wortsman, Ross Wightman, Cade Gordon, Nicholas Carlini, Rohan Taori, Achal Dave, Vaishaal Shankar, Hongseok Namkoong, John Miller, Hannaneh Hajishirzi, Ali Farhadi, and Ludwig Schmidt. Openclip, July 2021. URL <https://doi.org/10.5281/zenodo.5143773>. If you use this software, please cite it as below.
- [21] Gabriel Ilharco, Marco Tulio Ribeiro, Mitchell Wortsman, Suchin Gururangan, Ludwig Schmidt, Hannaneh Hajishirzi, and Ali Farhadi. Editing Models with Task Arithmetic, March 2023. URL <http://arxiv.org/abs/2212.04089>.
- [22] Xisen Jin, Xiang Ren, Daniel Preotiuc-Pietro, and Pengxiang Cheng. Dataless Knowledge Fusion by Merging Weights of Language Models, April 2023. URL <http://arxiv.org/abs/2212.09849>.
- [23] Jean Kaddour. Stop Wasting My Time! Saving Days of ImageNet and BERT Training with Latest Weight Averaging, October 2022. URL <http://arxiv.org/abs/2209.14981>.
- [24] Jonathan Krause, Michael Stark, Jia Deng, and Li Fei-Fei. 3D Object Representations for Fine-Grained Categorization. In *2013 IEEE International Conference on Computer Vision Workshops*, pages 554–561, December 2013. doi: 10.1109/ICCVW.2013.77. URL <https://ieeexplore.ieee.org/document/6755945>.
- [25] Daniel Lawson and Ahmed H. Qureshi. Merging Decision Transformers: Weight Averaging for Forming Multi-Task Policies, September 2023. URL <http://arxiv.org/abs/2303.07551>.
- [26] Yann Lecun, Le’ on Bottou, Yoshua Bengio, and Parick Haffner. Gradient-based learning applied to document recognition. *Proceedings of the IEEE*, 86(11):2278–2324, 1998. ISSN 00189219. doi: 10.1109/5.726791. URL <http://ieeexplore.ieee.org/document/726791/>.
- [27] Weishi Li, Yong Peng, Miao Zhang, Liang Ding, Han Hu, and Li Shen. Deep Model Fusion: A Survey, September 2023. URL <http://arxiv.org/abs/2309.15698>.
- [28] Xi Lin, Zhiyuan Yang, Xiaoyuan Zhang, and Qingfu Zhang. Pareto Set Learning for Expensive Multi-Objective Optimization.

- [29] Xi Lin, Hui-Ling Zhen, Zhenhua Li, Qing-Fu Zhang, and Sam Kwong. Pareto Multi-Task Learning. In *Advances in Neural Information Processing Systems*, volume 32. Curran Associates, Inc., 2019. URL https://proceedings.neurips.cc/paper_files/paper/2019/hash/685bfde03eb646c27ed565881917c71c-Abstract.html.
- [30] Chang Liu, Chenfei Lou, Runzhong Wang, Alan Yuhan Xi, Li Shen, and Junchi Yan. Deep Neural Network Fusion via Graph Matching with Applications to Model Ensemble and Federated Learning. In *Proceedings of the 39th International Conference on Machine Learning*, pages 13857–13869. PMLR, June 2022. URL <https://proceedings.mlr.press/v162/liu22k.html>.
- [31] Liyang Liu, Yi Li, Zhanghui Kuang, Jing-Hao Xue, Yimin Chen, Wenming Yang, Qingmin Liao, and Wayne Zhang. Towards Impartial Multi-task Learning. In *International Conference on Learning Representations*, October 2020. URL <https://openreview.net/forum?id=IMPnRXEWpvvr>.
- [32] Debabrata Mahapatra and Vaibhav Rajan. Multi-Task Learning with User Preferences: Gradient Descent with Controlled Ascent in Pareto Optimization. In *Proceedings of the 37th International Conference on Machine Learning*, pages 6597–6607. PMLR, November 2020. URL <https://proceedings.mlr.press/v119/mahapatra20a.html>.
- [33] Michael Matena and Colin Raffel. Merging Models with Fisher-Weighted Averaging, August 2022. URL <http://arxiv.org/abs/2111.09832>.
- [34] Aviv Navon, Aviv Shamsian, Gal Chechik, and Ethan Fetaya. Learning the Pareto Front with Hypernetworks, April 2021. URL <http://arxiv.org/abs/2010.04104>.
- [35] Yuval Netzer, Tao Wang, Adam Coates, Alessandro Bissacco, Bo Wu, and Andrew Y Ng. Reading Digits in Natural Images with Unsupervised Feature Learning. 2021.
- [36] Adam Paszke, Sam Gross, Francisco Massa, Adam Lerer, James Bradbury, Gregory Chanan, Trevor Killeen, Zeming Lin, Natalia Gimelshein, Luca Antiga, Alban Desmaison, Andreas Köpf, Edward Yang, Zach DeVito, Martin Raison, Alykhan Tejani, Sasank Chilamkurthy, Benoit Steiner, Lu Fang, Junjie Bai, and Soumith Chintala. PyTorch: An Imperative Style, High-Performance Deep Learning Library, December 2019. URL <http://arxiv.org/abs/1912.01703>.
- [37] Alec Radford, Jeffrey Wu, Rewon Child, David Luan, Dario Amodei, and Ilya Sutskever. Language Models are Unsupervised Multitask Learners. 1:9, 2019.
- [38] Alec Radford, Jong Wook Kim, Chris Hallacy, Aditya Ramesh, Gabriel Goh, Sandhini Agarwal, Girish Sastry, Amanda Askell, Pamela Mishkin, Jack Clark, Gretchen Krueger, and Ilya Sutskever. Learning Transferable Visual Models From Natural Language Supervision, February 2021. URL <http://arxiv.org/abs/2103.00020>.
- [39] Sebastian Ruder. An Overview of Multi-Task Learning in Deep Neural Networks, June 2017. URL <http://arxiv.org/abs/1706.05098>.
- [40] Sunny Sanyal, Jean Kaddour, Abhishek Kumar, and Sujay Sanghavi. Understanding the Effectiveness of Early Weight Averaging for Training Large Language Models, June 2023. URL <http://arxiv.org/abs/2306.03241>.
- [41] S. Schäffler, R. Schultz, and K. Weinzierl. Stochastic Method for the Solution of Unconstrained Vector Optimization Problems. *Journal of Optimization Theory and Applications*, 114(1): 209–222, July 2002. ISSN 1573-2878. doi: 10.1023/A:1015472306888. URL <https://doi.org/10.1023/A:1015472306888>.
- [42] Ozan Sener and Vladlen Koltun. Multi-Task Learning as Multi-Objective Optimization, January 2019. URL <http://arxiv.org/abs/1810.04650>.
- [43] J. Stallkamp, M. Schlipsing, J. Salmen, and C. Igel. Man vs. computer: Benchmarking machine learning algorithms for traffic sign recognition. *Neural Networks*, 32:323–332, August 2012. ISSN 0893-6080. doi: 10.1016/j.neunet.2012.02.016.

- [44] Anke Tang, Li Shen, Yong Luo, Liang Ding, Han Hu, Bo Du, and Dacheng Tao. Concrete Subspace Learning based Interference Elimination for Multi-task Model Fusion, December 2023. URL <http://arxiv.org/abs/2312.06173>.
- [45] Anke Tang, Li Shen, Yong Luo, Nan Yin, Lefei Zhang, and Dacheng Tao. Merging Multi-Task Models via Weight-Ensembling Mixture of Experts, February 2024. URL <http://arxiv.org/abs/2402.00433>.
- [46] Norman Tatro, Pin-Yu Chen, Payel Das, Igor Melnyk, Prasanna Sattigeri, and Rongjie Lai. Optimizing Mode Connectivity via Neuron Alignment. In *Advances in Neural Information Processing Systems*, volume 33, pages 15300–15311. Curran Associates, Inc., 2020. URL <https://proceedings.neurips.cc/paper/2020/hash/aecad42329922dfc97eee948606e1f8e-Abstract.html>.
- [47] Alex Wang, Amanpreet Singh, Julian Michael, Felix Hill, Omer Levy, and Samuel Bowman. GLUE: A Multi-Task Benchmark and Analysis Platform for Natural Language Understanding. In *Proceedings of the 2018 EMNLP Workshop BlackboxNLP: Analyzing and Interpreting Neural Networks for NLP*, pages 353–355, Brussels, Belgium, 2018. Association for Computational Linguistics. doi: 10.18653/v1/W18-5446. URL <http://aclweb.org/anthology/W18-5446>.
- [48] Thomas Wolf, Lysandre Debut, Victor Sanh, Julien Chaumond, Clement Delangue, Anthony Moi, Pierric Cistac, Tim Rault, Rémi Louf, Morgan Funtowicz, Joe Davison, Sam Shleifer, Patrick von Platen, Clara Ma, Yacine Jernite, Julien Plu, Canwen Xu, Teven Le Scao, Sylvain Gugger, Mariama Drame, Quentin Lhoest, and Alexander M. Rush. HuggingFace’s Transformers: State-of-the-art Natural Language Processing, July 2020. URL <http://arxiv.org/abs/1910.03771>.
- [49] Mitchell Wortsman, Gabriel Ilharco, Samir Yitzhak Gadre, Rebecca Roelofs, Raphael Gontijo-Lopes, Ari S. Morcos, Hongseok Namkoong, Ali Farhadi, Yair Carmon, Simon Kornblith, and Ludwig Schmidt. Model soups: Averaging weights of multiple fine-tuned models improves accuracy without increasing inference time, July 2022. URL <http://arxiv.org/abs/2203.05482>.
- [50] Jianxiong Xiao, James Hays, Krista A. Ehinger, Aude Oliva, and Antonio Torralba. SUN database: Large-scale scene recognition from abbey to zoo. In *2010 IEEE Computer Society Conference on Computer Vision and Pattern Recognition*, pages 3485–3492, San Francisco, CA, USA, June 2010. IEEE. ISBN 978-1-4244-6984-0. doi: 10.1109/CVPR.2010.5539970. URL <http://ieeexplore.ieee.org/document/5539970/>.
- [51] Prateek Yadav, Derek Tam, Leshem Choshen, Colin Raffel, and Mohit Bansal. Resolving Interference When Merging Models, June 2023. URL <http://arxiv.org/abs/2306.01708>.
- [52] Enneng Yang, Li Shen, Zhenyi Wang, Guibing Guo, Xiaojun Chen, Xingwei Wang, and Dacheng Tao. Representation Surgery for Multi-Task Model Merging, February 2024. URL <http://arxiv.org/abs/2402.02705>.
- [53] Le Yu, Bowen Yu, Haiyang Yu, Fei Huang, and Yongbin Li. Language Models are Super Mario: Absorbing Abilities from Homologous Models as a Free Lunch, November 2023. URL <http://arxiv.org/abs/2311.03099>.
- [54] David Yunis, Kumar Kshitij Patel, Pedro Savarese, Gal Vardi, Karen Livescu, Matthew Walter, Jonathan Frankle, and Michael Maire. On Convexity and Linear Mode Connectivity in Neural Networks. *OPT2022: 14th Annual Workshop on Optimization for Machine Learning*, 2022.
- [55] Matthew D. Zeiler and Rob Fergus. Visualizing and Understanding Convolutional Networks, November 2013. URL <http://arxiv.org/abs/1311.2901>.
- [56] Qingfu Zhang and Hui Li. MOEA/D: A Multiobjective Evolutionary Algorithm Based on Decomposition. *IEEE Transactions on Evolutionary Computation*, 11(6):712–731, December 2007. ISSN 1941-0026. doi: 10.1109/TEVC.2007.892759. URL <https://ieeexplore.ieee.org/document/4358754>.

- [57] Xiaoyuan Zhang, Xi Lin, Bo Xue, Yifan Chen, and Qingfu Zhang. Hypervolume Maximization: A Geometric View of Pareto Set Learning. *Advances in Neural Information Processing Systems*, 36:38902–38929, December 2023. URL https://proceedings.neurips.cc/paper_files/paper/2023/hash/7a7f6cc5dc2a84fb4edf0feb8e5cfd50-Abstract-Conference.html.
- [58] Yu Zhang and Qiang Yang. A Survey on Multi-Task Learning. *IEEE Transactions on Knowledge and Data Engineering*, pages 1–1, 2021. ISSN 1041-4347, 1558-2191, 2326-3865. doi: 10.1109/TKDE.2021.3070203. URL <https://ieeexplore.ieee.org/document/9392366/>.
- [59] Hongling Zheng, Li Shen, Anke Tang, Yong Luo, Han Hu, Bo Du, and Dacheng Tao. Learn From Model Beyond Fine-Tuning: A Survey, October 2023. URL <http://arxiv.org/abs/2310.08184>.

The appendix is organized into several sections, each providing additional insights and details related to different aspects of the main work.

A Proof of Existence of an Error Bound	15
B Task-Specific Model Acquisition	15
C Model Merging Baselines	16
D Pareto Optimal Learning Baselines	18
E Device Specifications	18
F Routing Analysis	19

A Proof of Existence of an Error Bound

Given a MOOP with T objectives, the Pareto front is defined as $\mathcal{P} = \{\mathcal{L}(\phi) \mid \phi \in \Phi \text{ and } \nexists \phi' \in \Phi \text{ s.t. } \phi' \prec \phi\}$, where $\mathcal{L}(\phi) = (l_1(\phi), \dots, l_T(\phi))$ is the vector of task-specific losses, and $\Phi = \mathbb{R}^{|\phi|}$ is the space of parameters ϕ for the upscaled module. The Pareto front estimated by the proposed MoE modules is defined as $\mathcal{P}_{\text{MoE}} = \{\mathcal{L}(\phi) \mid \phi \in \Phi_{\text{MoE}} \text{ and } \nexists \phi' \in \Phi_{\text{MoE}} \text{ s.t. } \phi' \prec \phi\}$.

Here we proof Theorem 4.1 as follows:

Proof. Let $\phi^* \in \Phi_{\text{MoE}}$ be any point on the approximated Pareto front \mathcal{P}_{MoE} . Since for the MoE Φ_{MoE} is a subspace of the full parameter space Φ , there exists a point $\phi \in \Phi$ that is closest to ϕ^* in Euclidean distance. That is,

$$\phi = \arg \min_{\phi' \in \Phi} \|\phi' - \phi^*\|_2. \quad (6)$$

Since the loss functions l_i are continuous, there exists an $\epsilon > 0$ such that

$$\|\phi^* - \phi\|_2 < \delta \implies \|l_i(\phi^*) - l_i(\phi)\|_2 < \epsilon \quad \forall i = 1, \dots, T. \quad (7)$$

By the triangle inequality, this implies

$$\|\mathcal{L}(\phi^*) - \mathcal{L}(\phi)\|_2 = \sqrt{\sum_{i=1}^T (l_i(\phi^*) - l_i(\phi))^2} \leq \sqrt{T}\epsilon. \quad (8)$$

Therefore, for any point $\mathcal{L}(\phi^*) \in \mathcal{P}_{\text{MoE}}$ on the Pareto front approximated by the MoE, there exists a point $\mathcal{L}(\phi) \in \mathcal{P}$ on the true Pareto front such that their Euclidean distance is bounded by $\sqrt{T}\epsilon$. \square

B Task-Specific Model Acquisition

Table 5: Individual performance of pre-trained and fine-tuned CLIP-ViT-B/32 models.

Model	SUN397	Cars	RESISC45	EuroSAT	SVHN	GTSRB	MNIST	DTD
pre-trained	63.2	59.6	60.2	45.0	31.6	32.6	48.3	44.4
SUN397	75.3	49.2	54.2	49.4	28.3	29.7	49.1	40.1
Cars	55.9	77.7	51.2	39.6	29.4	30.2	51.8	38.8
RESISC45	52.2	47.2	96.1	56.3	24.2	22.5	49.6	34.7
EuroSAT	51.6	45.3	32.5	99.9	19.3	26.1	37.9	35.9
SVHN	49.3	40.2	30.3	12.7	97.5	31.4	85.7	28.7
GTSRB	46.4	38.9	29.5	22.0	43.9	98.7	39.5	28.5
MNIST	49.2	40.2	33.5	20.7	49.2	15.3	99.7	27.4
DTD	50.4	49.4	41.9	33.9	28.9	22.8	47.8	79.4

Image Classification. For image classification tasks, we used the CLIP-ViT models [38] pre-trained on large-scale image-text datasets from OpenCLIP library [20]. Checkpoints of the fine-tuned models

Table 6: Individual performance of pre-trained and fine-tuned CLIP-ViT-L/14 models.

Model	SUN397	Cars	RESISC45	EuroSAT	SVHN	GTSRB	MNIST	DTD
pre-trained	68.2	77.9	71.3	61.3	58.4	50.6	76.4	55.4
SUN397	82.3	71.2	64.7	54.6	52.5	46.9	75.1	51.9
Cars	67.2	92.4	68.4	56.4	57.8	48.4	73.7	55.6
RESISC45	66.3	71.5	97.4	57.7	52.7	48.5	78.9	52.1
EuroSAT	65.7	70.8	46.9	99.9	49.1	46.6	75.0	48.4
SVHN	67.6	70.8	64.4	37.0	98.1	47.2	91.1	51.9
GTSRB	66.5	73.4	64.8	34.5	61.6	99.2	82.9	52.5
MNIST	68.5	73.0	65.5	43.4	66.5	44.1	99.7	52.6
DTD	66.0	74.4	68.0	55.7	51.3	47.8	64.3	84.1

are the same as those used in the Task Arithmetic paper [21], and are publicly available¹. In Tables 5 and 6, we provide the individual performance of the pre-trained and fine-tuned CLIP-ViT-B/32 and CLIP-ViT-L/14 models on the eight image classification tasks.

Table 7: Individual performance of pre-trained and fine-tuned GPT-2 models.

Model	MRPC	MNLI	COLA	SST-2	QNLI	QQP	RTE	Avg.
MRPC	80.4	25.9	30.8	49.1	47.1	65.9	49.1	49.8
MNLI	33.8	82.1	59.5	40.5	46.5	24.9	57.4	49.2
COLA	68.4	32.8	76.8	51.0	50.4	39.2	48.0	52.4
SST-2	40.2	32.9	51.8	91.2	49.8	56.8	44.4	52.4
QNLI	30.6	38.9	58.7	47.0	88.3	39.9	48.7	50.3
QQP	62.3	25.7	31.4	49.1	45.0	89.6	49.1	50.3
RTE	37.5	47.7	52.8	54.9	53.5	33.7	65.3	49.3

Natural Language Tasks. For natural language processing tasks, we used the pre-trained GPT-2 [37] from the Hugging Face Transformers library [48]. We fine-tuned the pre-trained GPT-2 model on the seven downstream tasks from the GLUE benchmark [47] for 3 epochs with a batch size of 8, the learning rate is set to 5×10^{-5} , and the Adam optimizer is used with weight decay of 10^{-9} . In Table 7, we provide the individual performance of the fine-tuned GPT-2 models on the seven natural language processing tasks and bold the best performance for each task.

C Model Merging Baselines

Here we provide a brief overview of the model merging baselines used in our experiments. We compare our approach with several established model merging techniques that aggregate knowledge from multiple models to enhance performance across different tasks. Below are the details of each baseline method:

1. **Simple Averaging:** This method merges the parameters of multiple models by taking the average of their weights.
2. **Fisher Merging [33]:** This approach combines models by taking the weighted average of their parameters based on the Fisher information matrix. For each fine-tuned model, compute the Fisher information matrix, which captures the importance of each model.
3. **RegMean [22]:** RegMean is a model merging technique for merging linear layers. RegMean operates by pre-computing the inner production matrices of training data for each individual model. When it comes to merging these models, the method retrieves the weights and inner product matrices from each model and computes new weights based on equation:

$$W_{\text{merged}} = \left(\sum_i X_i^\top X_i \right)^{-1} \sum_i (X_i^\top X_i W_i). \tag{9}$$

¹https://github.com/mlfoundations/task_vectors

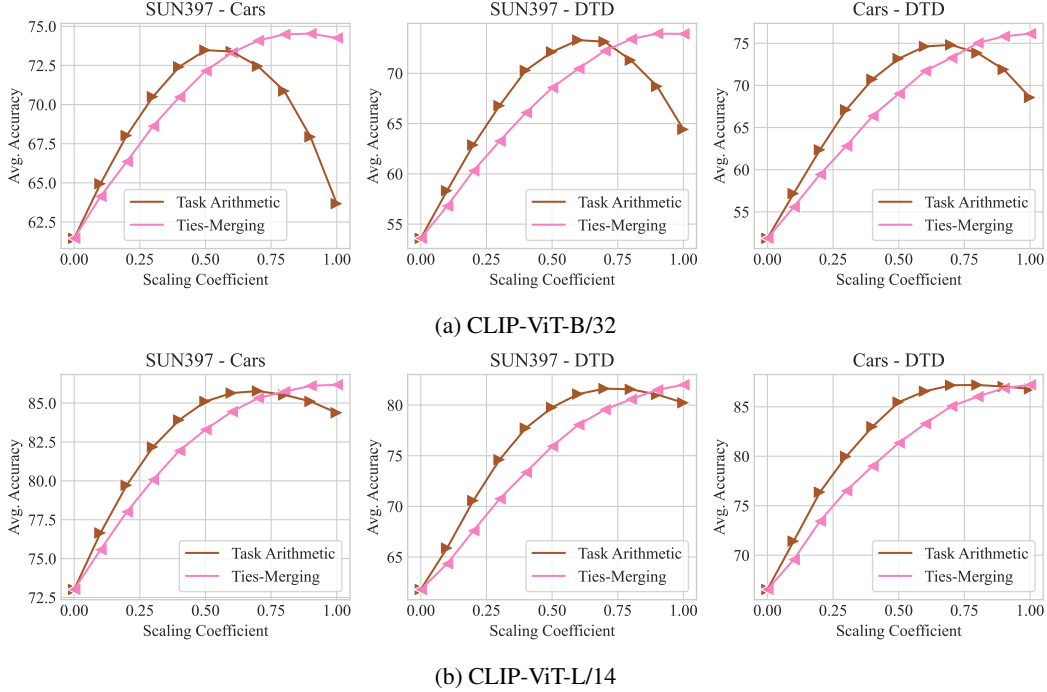


Figure 7: Merging two models for image classification tasks using Task Arithmetic and Ties-Merging. The horizontal axis represents scaling coefficients, and the vertical axis indicates the average accuracy of the merged model on the two tasks. It can be observed that for the two tasks scenario, Task Arithmetic roughly achieves the best performance around $\lambda = 0.6$, while Ties-Merging performs best at $\lambda = 1$.

4. **Task Arithmetic** [21]: For each model and task pair, we generate a task vector by taking the element-wise subtraction of the task-specific model and the pre-trained model within the parameter space. Subsequently, the task vectors from all models are summed up into a single vector, multiplied by a scalar factor, and added to the pre-trained model to obtain the merged model. Mathematically, the merging process can be represented as:

$$W_{\text{merged}} = W_{\text{pre-trained}} + \lambda \sum_i (W_i - W_{\text{pre-trained}}), \quad (10)$$

where λ is the scaling coefficient and W denotes the weights of the model.

5. **Ties-Merging** [51]: Ties-Merging is a model merging technique like Task Arithmetic, but it uses a different strategy to merge the task vectors. Instead of summing the task vectors, Ties-Merging takes a more nuanced approach. In Ties-Merging, the process starts with “Trimming”, discarding minor updates to the fine-tuned model’s parameters to reduce noise. Then, “Elect Sign” determines the sign of each parameter update based on its impact on task performance, resolving sign disagreements across the models either by majority vote or using an oracle sign vector. Lastly, “Merge” combines the parameter updates respecting the resolved signs, aiming to maintain the specialized learning from each task and create a multi-task model without additional fine-tuning.

These baseline methods serve as important benchmarks to assess the performance gains obtained by our proposed approaches. In particular, we investigate the performance of Task Arithmetic and Ties-Merging on the two-tasks scenario for CLIP-ViT-B/32 and CLIP-ViT-L/14 models in Figure 7. Because for these two methods, the performance of the merged model is highly dependent on the scaling coefficient λ , we plot the average accuracy of the merged model on the two tasks against the scaling coefficient λ . It can be observed that for the two-tasks scenario, Task Arithmetic roughly achieves the best performance around $\lambda = 0.6$, while Ties-Merging performs best at $\lambda = 1$. In our experiments, we report the best performance of each method on the validation set.

D Pareto Optimal Learning Baselines

Pareto set learning methods. There are many methods for learning the Pareto set of a multi-objective optimization problem, as introduced in Section 2. Some methods are theoretically solid and elegant. However, most of these methods demand significant computational resources and do not scale well to larger models. Typically, these methods are limited to benchmarking in multi-objective optimization problems with 2-3 closed-form objective functions. Therefore, we do not compare with these methods in our experiments. In this work, we focus on the Pareto optimal learning methods that can be applied to large-scale neural networks, such as linear scalarization, EPO search and MGDA.

1. **Linear Scalarization.** This method involves combining the multiple objectives into a single objective function by assigning a weight to each objective. The weights are usually determined based on the importance of each objective. The combined objective function is then optimized using standard optimization techniques. However, this method can only find solutions that lie on the convex hull of the Pareto front. The single objective function is defined as follows:

$$l_{LS} = \sum_{i=1}^T r_i l_i(x), \tag{11}$$

where $l_i(x)$ is the i -th objective function, r_i is the weight assigned to the i -th objective, and T is the number of objectives.

2. **EPO Search [32].** The Exact Pareto Optimal (EPO) search is also a method that aims to find a single Pareto optimal solution. Unlike linear scalarization, EPO search can find solutions that are exactly Pareto optimal with respect to given preference vector. Where the non-uniformity of the objective values is taken into account, which is defined as follows:

$$\text{Non-uniformity} = \text{KL} \left(\hat{l} \middle| \frac{1}{T} \right). \tag{12}$$

Where \hat{l} is the weighted normalization of the objective values, and T is the number of objectives.

$$\hat{l}_i = \frac{r_i l_i}{\sum_{j=1}^T r_j l_j} \tag{13}$$

3. **MGDA.** The Multiple Gradient Descent Algorithm (MGDA) is a method that uses the gradients of the objective functions to find a direction that improves all objectives simultaneously. In our experiments, we compare the performance of our proposed methods with these Pareto optimal learning baselines. The results show that our methods can achieve comparable or better performance, demonstrating their effectiveness in MOOPs.

E Device Specifications

All experiments were carried out on a server with 4 NVIDIA 4090 GPUs, each with 24GB of memory, using PyTorch [36] and Hugging Face Transformers [48] libraries.

Computational burden. The computational burden of different methods can be influenced by several factors, including the number of trainable parameters, the number of objectives, and the size of the model. In our experiments, we compare the computational burden of our proposed methods with the Pareto optimal learning baselines, including linear scalarization (LS), EPO search, and MGDA. In Table 8, we summarize the training details for the Pareto set approximation experiments with image classification tasks. Empirically, it is observed that the computational burden can be arranged as follows: Ours-LS(MLP) < Ours-EPO(MLP) < LS < Ours-LS(Attn+MLP) < Ours-EPO(Attn+MLP) < EPO < MGDA. The EPO method, on the other hand, tends to have a higher computational burden because we use a CPU implementation of the EPO method, leading to longer training time, which can be further optimized.

Efficiency of the proposed methods. The low computational burden of the proposed methods can be attributed to the efficient nature of the weight-ensembling mixture of experts (MoE) structure. This structure allows for tuning only a small number of parameters to capture the trade-offs between multiple objectives. By ensembling the weights of specialized single-task models, the MoE module

Table 8: Summarization of training details for Pareto set approximation experiments with image classification tasks. We use Adam optimizer for all experiments. The training time is measured on NVIDIA 4090 GPUs with 24GB memory. We utilize a CPU implementation of the EPO method, leading to longer training time. This can be further optimized.

Method	#Tasks	#Trainable / #Total	Batch Size (each)	GPU usage	Wall Time
<i>CLIP-ViT-B/32, 113.45M params.</i>					
LS	2	113.45M / 113.45M	16	3.4GB	≈ 4 mins
EPO	2	113.45M / 113.45M	16	6.1GB	≈ 8 mins
Ours-LS	2	264 / 226.79M	16	2.8GB	≈ 2-3 mins
Ours-LS (All)	2	1.43K / 338.88M	16	3.9GB	≈ 3 mins
Ours-EPO	2	264 / 226.79M	16	3.1GB	≈ 3-4 mins
Ours-EPO (All)	2	1.43K / 338.88M	16	3.9GB	≈ 5-6 mins
Ours-LS	3	540 / 283.46M	16	3.6GB	≈ 3 mins
Ours-EPO	3	540 / 283.46M	16	3.9GB	≈ 5 mins
LS	8	113.45M / 113.45M	16	7.4GB	≈ 13 mins
Ours-LS	8	3.36K / 566.81M	16	7.4GB	≈ 10 mins
Ours-LS (All)	8	18.20K / 1.02B	16	10.0GB	≈ 8 mins
Ours-EPO	8	3.36K / 566.81M	16	7.8GB	≈ 30 mins
Ours-EPO (All)	8	18.20K / 1.02B	16	10.5GB	≈ 85mins
<i>CLIP-ViT-L/14, 342.56M params.</i>					
EPO	2	342.56M / 342.56M	16	4×20.5GB (DDP)	
MGDA	2	342.56M / 342.56M	16	2×20.5GB (DDP)	≈ 80 mins
Ours-LS	2	528 / 745.46M	16	19.8GB	≈ 16 mins
Ours-EPO	2	528 / 745.46M	16	20.8GB	≈ 37 mins
Ours-LS	8	6.72K / 1.95B	12	4×21.5GB (DDP)	≈ 15 mins
Ours-EPO	8	6.72K / 1.95B	12	4×22.1GB (DDP)	≈ 85 mins

can provide a close approximation of the entire Pareto set of large neural networks, thus reducing the computational demand and memory consumption compared to other methods. This efficiency makes the approach scalable to both the number of objectives and the size of the model, making it a practical solution for multi-objective optimization problems in deep learning.

F Routing Analysis

To better understand the routing mechanism in the weight-ensembling Mixture of Experts (MoE) modules, we analyze the expert routing weights associated with different preference vectors using CLIP-ViT-B/32 (Ours-LS, MLP only). For each unit preference vector, we compute the routing weights at various depths for the MoE routers and present these weights in Figure 8. We observe the following key points:

- **Variability across depths:** The routing weights exhibit significant variation across different depths of the model. According to the empirical findings of previous research [55], at various depths, the model processes information at different levels of abstraction. In early layers, the model may focus on low-level features like edges and textures, while in later layers, it may capture more complex and high-level concepts. This variation in the level of abstraction can lead to differences in the routing weights across depths.
- **Specificity to tasks:** Each preference vector, associated with a specific task, directs the routing towards relevant experts at higher depths. This demonstrates the model’s capability to adapt its weights based on the preference vector, validating the intended behavior of MoE to specialize expert usage for each task.
- **Expert utilization:** Some experts are more frequently utilized across different preference vectors, and this usage varies at different depths. For example, the ‘Cars’ expert is frequently employed in early layers, indicating its effectiveness in extracting basic image features. In contrast, the ‘DTD’ expert is often used in later layers, suggesting its specialization in deeper contextual understanding.



Figure 8: Visualization of routing weights for different preference vectors using CLIP-ViT-B/32. The preference vector for a specific task is denoted as r_{task} , with a value of one, and zeros for others.